

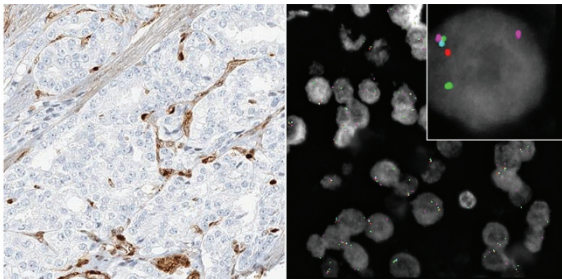
## INSIDE THE USCAP JOURNALS

doi:10.1038/modpathol.2016.120

### MODERN PATHOLOGY

#### Analytic validation of PTEN immunohistochemistry

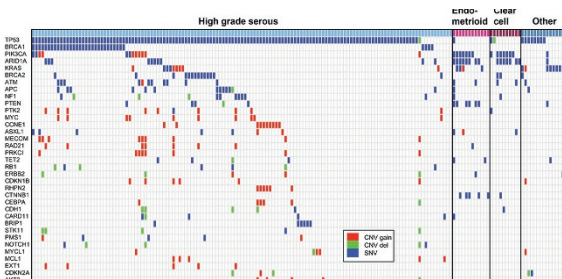
See page 904



With the loss of PTEN emerging as a promising biomarker of prostate cancer, Lotan *et al* developed a clinical-grade four-color fluorescence *in situ* hybridization (FISH) assay for the detection of *PTEN* locus loss. In a multi-institutional cohort of 731 prostate tumor samples, the assay was 91% specific for the absence of the *PTEN* gene, while the negative predictive value for intact PTEN immunohistochemistry was 96% for lack of any gene deletion and 99.6% for lack of homozygous *PTEN* deletion. The assay needed to be examined for discrepancies between immunohistochemistry and FISH, some of which were hypothesized to be due to focal tumor areas with *PTEN* gene deletion that were missed or not analyzed by FISH in blinded assays. With more defined and well-validated antibodies against PTEN, the application of this promising biomarker becomes a method for establishing PTEN as a prognostic and potentially predictive biomarker in the clinic.

#### Molecular alterations in extrauterine carcinoma

See page 893



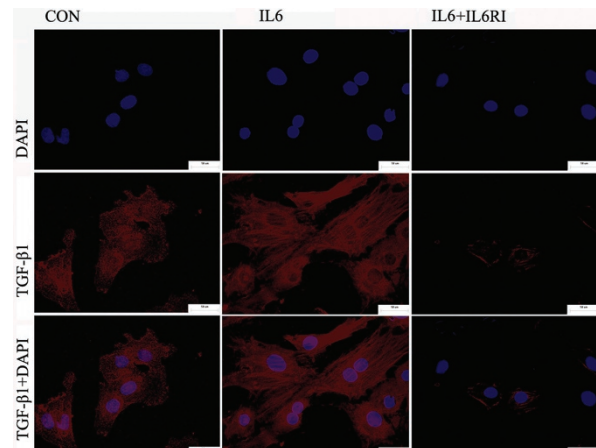
Germline *BRCA* mutations have been shown to result in characteristic histologic and architectural patterns in high-grade extrauterine serous carcinomas. Ritterhouse *et al* investigated the molecular patterning of this type of tumor among 174

carcinomas of the fallopian tube, ovary, or peritoneum. They used targeted next-generation sequencing on isolated DNA to look at single-nucleotide and copy-number variants. Overall, 138 (79%) of the tumors were classified as high-grade serous carcinoma, and the most common somatic mutations in high-grade serous carcinomas were *TP53* (94%), *BRCA1* (25%), *BRCA2* (11%), and *ATM* (7%). Thus, most of the mutations were in genes involving DNA-repair pathway genes. Because homologous recombination-deficient tumors depend on Polθ/PARP1-mediated alternative end-joining repair, the authors hypothesize that PARP inhibitors will benefit many women with these types of tumors.

### LABORATORY INVESTIGATION

#### Investigating the postmyocardial infarction microenvironment

See page 839

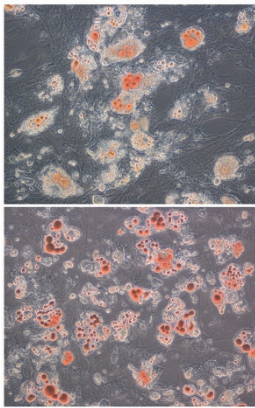


Wang *et al* sought to investigate the role of interleukin-6 (IL-6) in myocardial fibrosis using fibroblasts, cardiomyocytes, and blood vascular endothelial cells from the ventricles of neonatal rats. The authors hypothesized that overexpression of IL-6 was sufficient to induce myofibroblastic proliferation via transforming growth factor-β1 (TGF-β1)-mediated MMP2/MMP3 signaling. They propose that this pathway promotes conversion and fibrosis of fibroblasts under hypoxic conditions. They showed that IL-6 activated Caspase3 and Smad3 from the apoptosis pathway and reduced expression of Bcl2, which resulted in apoptosis of cardiomyocytes under hypoxic coculture. Fibroblasts overexpressing IL-6 also promoted angiogenesis in vascular endothelial cells under hypoxia. Since a hypoxic microenvironment prevails with myocardial infarction, the authors propose that upregulation

of IL-6 promotes proliferation and collagen formation from fibroblasts, apoptosis in cardiomyocytes, and angiogenesis. Thus, IL-6 could be a candidate marker for myocardial remodeling via TGF- $\beta$ 1-mediated signaling pathways.

## Role of AT<sub>2</sub>R in adipogenesis

See page 909



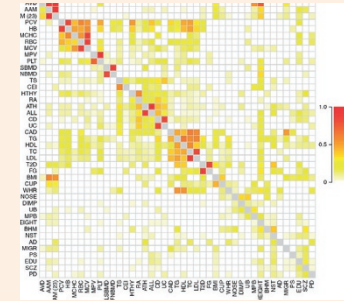
A study of metabolic syndrome and the role of the renin-angiotensin system (RAS) and mesenchymal stem cells led Matsushita *et al* to investigate the specific role for AT<sub>2</sub>R in adipogenesis. Using AT<sub>2</sub>R-null mouse mesenchymal stem cells (MSCs), the authors sought to determine how the receptor affected differentiation of MSCs to adipocytes. AT<sub>2</sub>R-null cells showed significantly greater adipocytic differentiation compared with wild-type cells, as assessed via lipophilic fluorescent dye. Using quantitative RT-PCR, the investigators also examined the effect of AT<sub>2</sub>R deletion on expression of other genes. AT<sub>2</sub>R deletion resulted in increased expression of adipogenic marker genes (PPAR- $\gamma$ , fatty acid synthase, and adiponectin) and decreased expression of Wnt10b (known to inhibit adipogenesis) and cellular  $\beta$ -catenin (confirming the suppression of Wnt10b/ $\beta$ -catenin signaling). This suggests that the inhibitory effect of AT<sub>2</sub>R on adipogenesis in the authors' model was associated with, and perhaps mediated by, Wnt10b/ $\beta$ -catenin signaling.

MODERN PATHOLOGY (2016) 29, 786–787

## nature.com/pathology

### Shared genetic influence on human traits

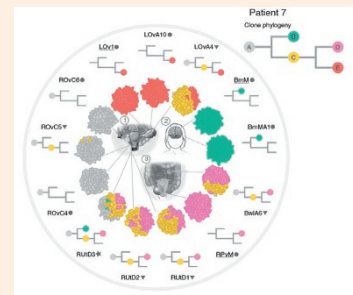
As reported in *Nature Genetics*, Pickrell *et al* utilized data from large genome-wide association studies to investigate not only the genetic variation behind one specific human trait, such as the risk of schizophrenia, but also whether they could identify sequences involved in several different traits. For instance, they attempted to identify genetic variants that increased risk of both schizophrenia and inflammatory bowel disease. They made note of the sheer number of genetic variants that influenced multiple traits while not having a consistent correlation in effect sizes. For example, they found that many autoimmune- and immune-related traits, as well as lipid, red cell, and immune traits, share a genetic cause without a consistent influence on the direction of the effect. More investigation of the method will be needed to rule out the possibility that this is simply because the method does not detect correlations in effect sizes or that environmental factors are not being properly accounted for.



*Nature Genetics* 2016;48:709–717; doi:10.1038/ng.3570

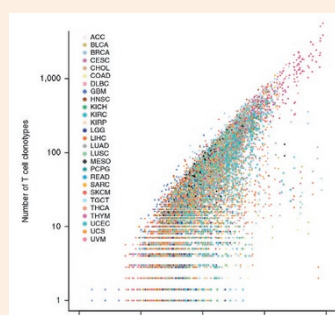
### Heterogeneity in spread of high grade serous ovarian carcinoma

In a phylogenetic analysis reported in *Nature Genetics*, McPherson *et al* examined 68 samples from seven patients with high-grade serous ovarian cancer to search for and identify constituent clones and their abundance. Using whole-genome and single-nucleus sequencing, the authors identified mutation loss as well as temporal activation of mutational processes that patterned clonal progression. In each patient, at least one site was composed polyphyletic clones rather than the clonally pure sites usually encountered. Clonal genotypes were used to infer clone phylogenies and even to investigate the order of mutation accumulation. Referring to the distribution of mutations in known ovarian cancer driver genes, the authors showed that *TP53* mutation was present in all clones, and *CDK12*, *BRCA2*, and *FAT3* mutations were detected in individual patients. This investigation supports the drive to further dissect the biological mechanisms and evolutionary selection contributing to the invasive capacity of ovarian cancers.



*Nature Genetics* 2016;48:758–767; doi:10.1038/ng.3573

### Infiltrating T-cell repertoire in human cancer



To analyze paired-end RNA-seq applied to 9,142 samples from The Cancer Genome Atlas (TCGA), Li *et al* developed a computational model for *de novo* assembly of sequences from CDR3 regions. Searching more deeply into the T cell-receptor repertoire of the tumor microenvironment than previously possible, they observed the interactions between tumors and the host immune system, yielding findings with a potential impact on selection of therapeutic targets. They demonstrated that the presence of cancer antigens, including those derived from somatic mutations and cancer/testis genes, might increase the diversity of the infiltrating T-cell repertoire. Indeed, they showed that the diversity of T-cell clones varies directly with the somatic mutation load across the >33 cancer types represented in the TCGA. The authors propose SPAG5 and TSSK6 as candidates for cancer vaccines. They anticipate that further analyses of tumor-immune interactions with more high-quality RNA could lead to even more detailed biological insights for future therapies.

*Nature Genetics* 2016;48:725–732; doi:10.1038/ng.3581

Emma Judson contributed to these reviews.